INTERNATIONAL JOURNAL FOR NUMERICAL METHODS IN FLUIDS, VOL. 21, 571–590 (1995)

VELOCITY CHARACTERISTICS OF STEADY FLOW THROUGH A STRAIGHT GENERIC INLET PORT

A. CHEN, K. C. LEE AND M. YIANNESKIS*

Centre for Heat Transfer and Fluid Flow Measurement, Department of Mechanical Engineering, King's College London, Strand, London WC2R 2LS, U.K.

AND

G. GANTI

Ford Motor Company Limited, Research and Engineering Centre, Laindon, Basildon, Essex SS15 6EE, U.K.

SUMMARY

This paper presents a combined experimental and computational study of the steady flow through an internal combustion engine inlet port. The port was of generic design with a straight centreline. The three-dimensional velocity and turbulence fields in the port and cylinder were simulated using a computational fluid dynamics programme. Laser sheet flow visualization and laser Doppler anemometry were also employed to investigate the flows and assess the predictions. The results show that a large-scale flow structure is created in the cylinder by the inlet jet and its interaction with the valve and cylinder walls. Both predictions and measurements show that the flow is strongly dependent on the valve lift but is not affected by the flow rate. Comparisons of the numerical predictions with the experimental data indicated that the mean flow features are accurately predicted in many parts of the flow field; some discrepancies are evident and stem primarily from the failure of the simulation to predict a small recirculation region in the port which affects the trajectory of the annular jet entering the cylinder. Calculations were also made without modelling the port shape by using simplified inlet conditions upstream of the valve seat. It was found that this approximation can provide a reasonable, albeit less accurate, description of the flow, but modelling of the port shape is necessary for accurate flow predictions.

KEY WORDS: CDF; predictions; laser Doppler anemometry; inlet port; cylinder; turbulence; steady flow

1. INTRODUCTION

In-cylinder air motion has long been recognized as being important for combustion efficiency and consequently for internal combustion engine performance. With numerous design modifications being introduced in practice to meet increasingly stringent emission requirements, all factors affecting the combustion process must be optimized. As a result, it is necessary that due attention is paid to the air motion. In particular, as the volumetric efficiency of an engine is affected by the inlet port design and engine speed,[1] it is necessary to improve the understanding of the effect of these parameters on the flow field inside the engine cylinder in order to optimize the characteristics of the intake air flow. For example, a number of studies have identified the roles of swirl and tumble[2] and of valve lift[3] on the generation of turbulence, particularly near TDC of compression.

The study of engine flows necessitates unsteady flow measurements and predictions, which are time-consuming and of considerable complexity. However, it has long been established that the quasi-steady flow assumption is valid for many parts of the induction stroke.[4] Therefore steady flow studies can

* Author to whom correspondence should be addressed.

CCC 0271–2091/95/070571–20

Received November 1994
Revised March 1995

provide useful data on port performance at a fraction of the computational and experimental cost before more complex unsteady flow studies are undertaken.

Computational fluid dynamics (CFD) has been employed in many investigations to predict the effects of the inlet port/valve configuration on the flow motion in internal combustion engines, in order to explore the levels and distributions of swirl and/or tumble produced and to determine whether they have an important influence on engine performance. Because of the complexity of the shapes of the port surface and of the valve and the necessity to form complex numerical grids around the valve stem, many simplifications have been made, for example by not modelling the inlet port and valve[2,3,5] or the valve stem.[6,7]

These simplifications have been necessitated by the complexity of inlet port shapes and the associated long time that is required to generate computational meshes that model port designs accurately. However, with the rapid development of computer technology and the associated improvements in computational speed and storage capacity, the capabilities of CFD codes have been increasing significantly. It is now feasible to generate computational meshes for many practical engine configurations for numerical simulation purposes.[8,9] Nevertheless, there are relatively few published studies of three-dimensional flow predictions validated by detailed experimental data.

One of the main reasons for the lack of suitable experimental data is that probe methods are obtrusive and interfere significantly with the flows in the narrow passages of inlet ports, while optical methods cannot be used owing to the complex shape of the port surface and the resulting refraction/dispersion of light beams at the port walls. Consequently, most investigations of flows through ports have dealt only with the in-cylinder flow structure. However, the above problem has been overcome[10,11] by using a refractive-index-matched fluid with port replicas made of transparent acrylic plastic: in this way the laser beams suffer no deflection at the port walls and laser Doppler anemometry (LDA) measurements can be made even through rough surfaces. These investigations have been concerned with both idealized geometries, such as an axisymmetric port,[10] and production designs[11] and have identified changes in the flow pattern with valve lift which varied for different port designs.

This paper describes a combined experimental and numerical investigation of the three-dimensional steady flow through an internal combustion engine with a generic straight port. The CFD predictions, the laser sheet flow visualization and the LDA measurements provided a detailed and accurate description of the characteristics of the flow induced by the port.

The effects of valve lift and mass flow rate on the velocity and turbulence characteristics were also investigated, as it is known that the pattern of the flow through the valve may vary with valve lift[12] and that volumetric efficiency is affected by engine speed (and, correspondingly, flow rate for steady flows). Two characteristic valve lifts, intermediate, 6 mm, and high, 10 mm, were selected in this work. In order to determine whether accurate flow predictions could be made without modelling the flow through the entire port, some of the calculations were performed with simplified inlet conditions upstream of the valve seat. In an attempt to quantify the turbulence-producing characteristics of every configuration studied in this work, the average level of turbulence kinetic energy was calculated from the CFD results. Detailed comparisons between the predictions and the experimental data are made to establish the accuracy of the CFD results and identify means of improving the calculations.

2. FLOW CONFIGURATION

The configuration of the inlet port, valve and cylinder is shown in Figure 1. The port axis is offset from the cylinder axis by 4·00 mm in the x-direction and 21·87 mm in the y-direction. The cylinder bore is $D = 93{\cdot}65$ mm and the valve diameter is $d = 43{\cdot}00$ mm.

In order to enable LDA measurements and flow visualization to be obtained in all parts of the flow

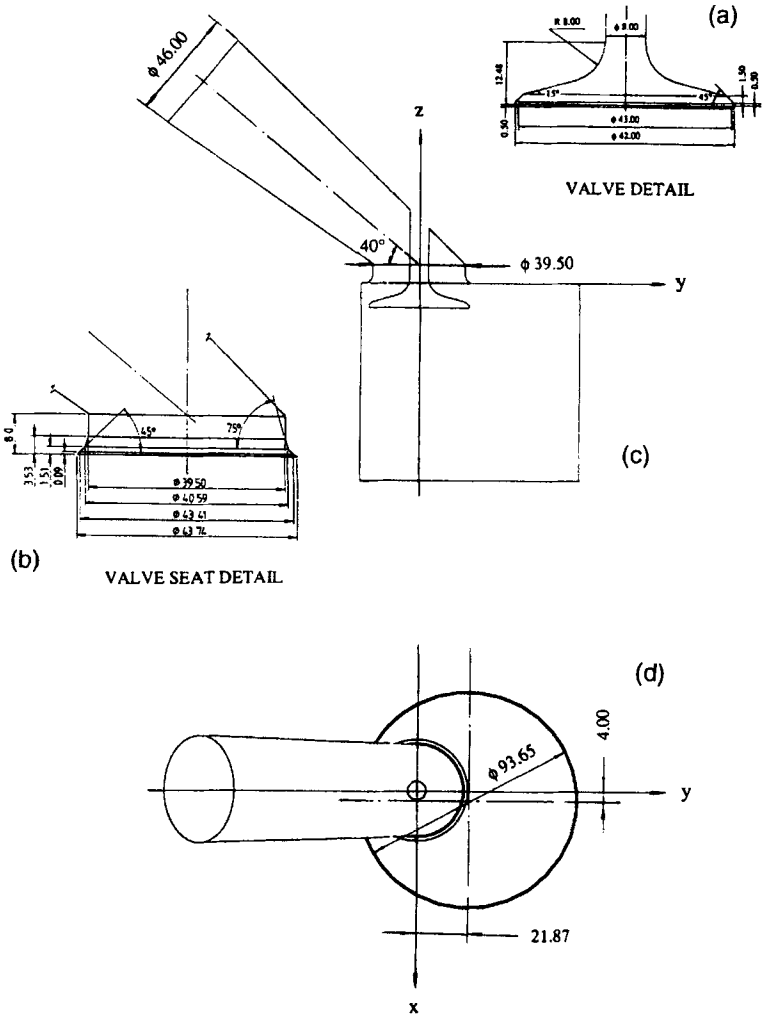

Figure 1. Inlet port, valve and cylinder configuration (all dimensions in millimetres): (a) valve detail; (b) valve seat detail; (c) elevation; (d) plan view

field and especially inside the port, a refractive-index-matching technique was employed in the experiments. A replica of the inlet port, valve, valve guide and cylinder was manufactured out of transparent acrylic plastic in the manner described in Reference 13. The working fluid was a mixture of oil of turpentine and tetraline in the volume ratio 69·2 : 30·8. Its density and kinematic viscosity were 894 kg m^{-3} and $1{\cdot}71 \times 10^{-6}$ m^2 s^{-1} respectively. The refractive index of the fluid was identical with that of the acrylic plastic at a temperature of 25 °C. In order to ensure accurate matching of the refractive indices, the temperature of the fluid mixture was held constant to within $\pm 0{\cdot}05$ °C by a proportional temperature control system. The similarity of the gas and liquid flows through inlet ports under incompressible flow conditions has been demonstrated previously.[11]

Detailed LDA measurements were obtained for valve lifts of 6 and 10 mm with a mass flow rate of 1·379 kg s^{-1}. The corresponding Reynolds number based on the diameter of the port inlet, 46 mm, and the bulk velocity at the inlet was 25,760. CFD predictions were performed with a mass flow rate of 1·379 kg s^{-1} for the 6 and 10 mm valve lifts and also with flow rates of 0·898 and 1·539 kg s^{-1} for the 10 mm lift.

The co-ordinate system employed in the present work is also shown in Figure 1. The origin of the co-ordinates is located on the valve axis at the elevation of the cylinder head surface. The mean and RMS velocity components in the directions x, y and z are denoted by U and u', V and v', and W and w' respectively.

3. COMPUTATIONAL MODEL

The predictions were performed using the CFD programme STAR-CD.[14] The k–ε model[15] was used to represent the flow turbulence. At all solid surfaces a 'law-of-the-wall' formulation was employed. The SIMPLE solution algorithm[16] was employed with an upwind differencing scheme. The computational grid contained 78,744 and 77,260 cells for the 6 and 10 mm valve lift predictions respectively. Figures 2(a) and 2(b) show the main part of the computational grid structure. Highly concentrated grid lines were located in the vicinity of the valve and in the regions of steep velocity gradients around the intake jet. The complex geometry of the port was modelled in detail using the mesh generation facilities of the preprocessor of the CFD code. The mesh was generated using a cell layer method; this involved the creation and manipulation of individual vertices and the attachment of cells to the vertices. The finite volume grid was body fitted and each cell was carefully designed to avoid inappropriate deformation and to ensure it was right-handed.

An inlet plenum was modelled upstream of the inlet plane of the port to alleviate the need for measurements of the inlet conditions. The velocity distribution specified at the inlet plane of the plenum chamber was a uniform mean velocity profile based on the mass flow rate for the simulation concerned. The turbulence intensity specified at that plane was 5% and the length scale specified was 10% of the diameter of the inlet plane of the port (i.e. 4·6 mm). The cylinder length was arranged to be six times the cylinder bore in order to ensure that the effects of recirculation regions under the valve were taken into account in full. An outlet boundary condition was defined at the exit plane of the cylinder: the gradients of all the variables along the mesh lines intersecting the exit plane were set to be zero. The flow velocities at the outlet boundary were specified to be directed away from the cylinder head.

The grid independence of the solutions obtained with the mesh models described above was determined through grid sensitivity tests, by increasing the numbers of cells, first by 25% and then by

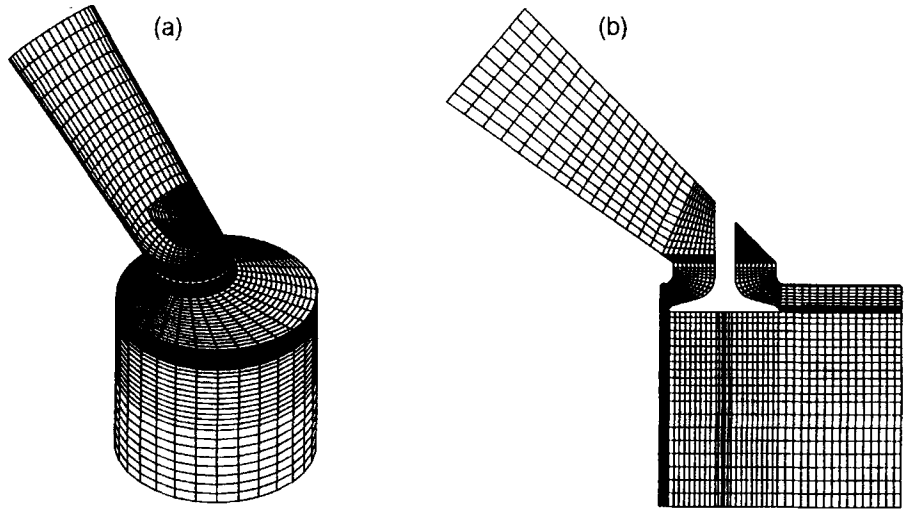

Figure 2. Computational grid structure: (a) general arrangement; (b) grid structure in $x = 0$ mm plane

50%. Differences in the results with the three meshes were smaller than the convergence criteria set in the predictions and it was therefore established that the solutions are independent of grid size.

In order to characterize the overall level of turbulence produced by the port under different valve lift and flow rate conditions, volume-averaged values of the kinetic energy of turbulence, $\bar{k}$ were calculated from the predicted values of k. For each case studied, the value of k at the centre of each cell in the mesh was weighted by the volume of the cell and the arithmetic average of all the weighted values was calculated. This enabled an average value of k to be obtained, for comparison purposes, for each flow configuration.

4. EXPERIMENTAL TECHNIQUES

Laser sheet flow visualization was carried out first in order to determine qualitatively the mean features of the flow and to identify regions where LDA measurements should be made. Various cross-stream and streamwise planes in the flow field were illuminated with a sheet of laser light generated with a 1·5 W argon ion laser and a combination of cylindrical and plano-convex lenses. Small air bubbles of mean diameter around 30 μm were generated in the flow to act as light scatterers. The bubble rise velocity was small enough in comparison with the flow velocities so that the bubbles could follow faithfully the mean flow patterns. The bubble streakline patterns were recorded by means of still and video cameras.

Measurements of the three mean velocity components and of the associated RMS fluctuations or turbulence levels were obtained by laser Doppler anemometry. The anemometer was of dual-beam, fringe type and operated in near-forward scatter. It comprised a 10 mW He–Ne laser, a diffraction grating for splitting the laser beam and providing a frequency shift between the two first-order beams, a photomultiplier and associated optics. A frequency counter interfaced to a computer was used to bandpass filter, amplify and process the Doppler signals. Naturally occurring contaminants in the fluid provided a sufficient number of scattering particles and therefore artificial seeding of the flow was not necessary. The quality of the Doppler signals was monitored constantly on an oscilloscope. The length and diameter of the LDA measuring volume were 423 μm and 65 μm respectively. The overall errors in the mean and RMS velocity measurements have been estimated to be approximately 5% and 10% respectively.[10,11]

5. RESULTS AND DISCUSSION

In the following subsection the characteristics of the mean flow produced with the 6 mm valve lift are described in detail in order to identify all the main flow features. Subsequently the mean flow structure generated with the 10 mm valve lift is described and compared with the 6 mm results in order to establish the effect of lift on the mean flow. Both sets of results are assessed by comparison with the LDA data. The predicted distributions of turbulence kinetic energy with the 6 and 10 mm valve lifts are then described and comparisons are made against the experimental data. Subsequently the effect of mass flow rate and predictions made without modelling the port shape are discussed.

Mean flow structure, 6 mm valve lift

Velocity vectors drawn from the LDA measurements of the mean velocity components V and W are shown in Figure 3 for the 6 mm valve lift. It can be observed that near the middle of the port the flow follows a direction parallel to the port centreline. As the flow approaches the valve stem, it is redirected towards the cylinder. On the left side of the port the formation of a small recirculation region in the vicinity of the wall above the valve seat was observed in the flow visualization, but the velocity vectors

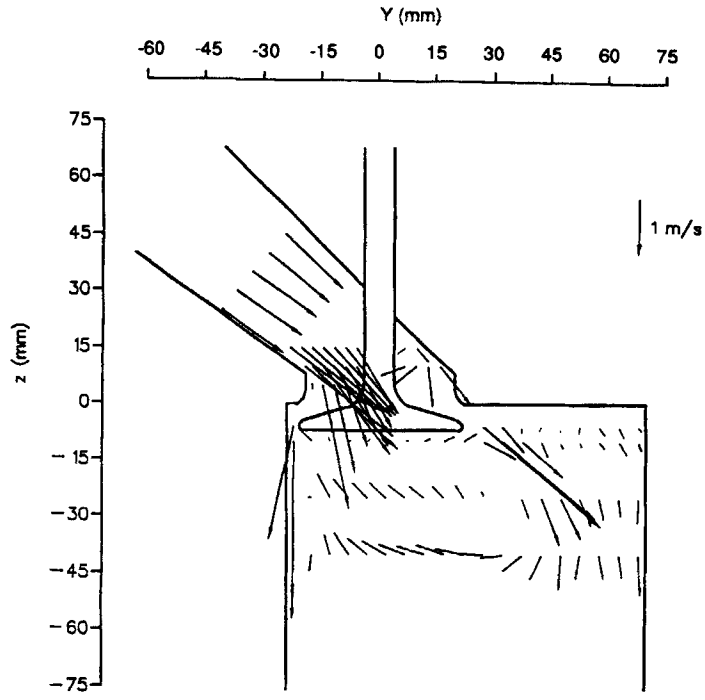

Figure 3. Measured mean velocity vectors in $x = 0$ mm plane ($L = 6$ mm, $Re = 25{,}760$)

measured in that location are of too small a magnitude to be distinguished in this figure. The flow accelerates strongly on the left side of the stem as it discharges into the cylinder.

The flow enters the cylinder as an annular conical jet of high velocity. It impinges on the cylinder wall nearest to the valve (on the left side) and is directed downwards to form a strong wall jet. This jet interacts with the flow emerging from the right side of the valve, resulting in the formation of an elongated counterclockwise-rotating vortex. On the right side of the cylinder the jet enters at an angle of 38° to the cylinder head. Downstream of the valve curtain area the jet forms a clockwise-rotating vortex which, together with that produced on the left side, comprises a three-dimensional ring vortex about $0{\cdot}75D$ in diameter situated below the valve.

It can be seen that all the major flow features observed above have been reproduced in the numerical simulations shown in Figure 4. The detail of the predictions allows flow features which were not evident in the LDA results to be determined. In the port, upstream of the valve stem, the flow accelerates without separation and is directed towards the valve stem. The predictions did not reproduce the small recirculation area adjacent to the wall above the valve seat and this will be discussed later. The flow directions on the right side of the stem are very similar to the measured ones. The detailed vectors shown in this figure indicate more clearly than the LDA data the presence of a flow separation in the wake of the valve stem, caused by a region of adverse pressure gradient behind the stem.

On the left side of the cylinder in Figure 4 a small recirculation is formed immediately after the valve seat. The jet flow on the right side of the valve enters the cylinder at an angle to the cylinder head very similar to that shown by the LDA results. This angle is smaller than the angle formed between the port axis and the cylinder head by 2°.

Figures 5 and 6 illustrate the measured and predicted mean velocity vectors respectively in a horizontal plane located 25 mm below the cylinder head. Both figures show the same flow pattern: the

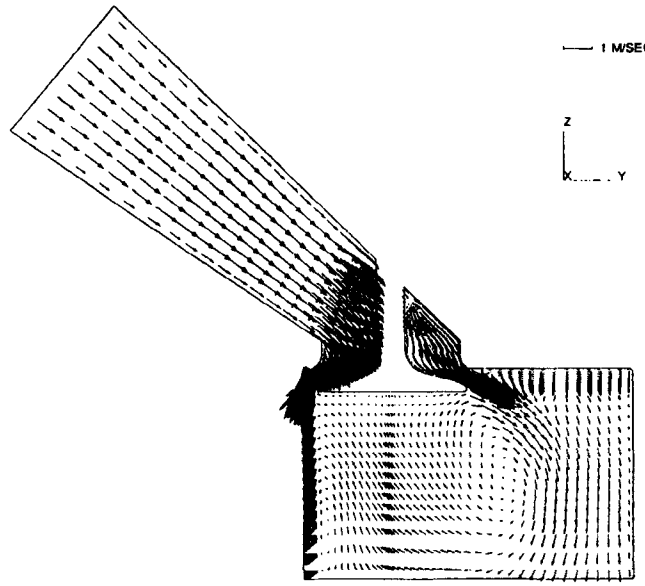

Figure 4. Predicted mean velocity vectors in $x = 0$ mm plane ($L = 6$ mm, $Re = 25{,}760$)

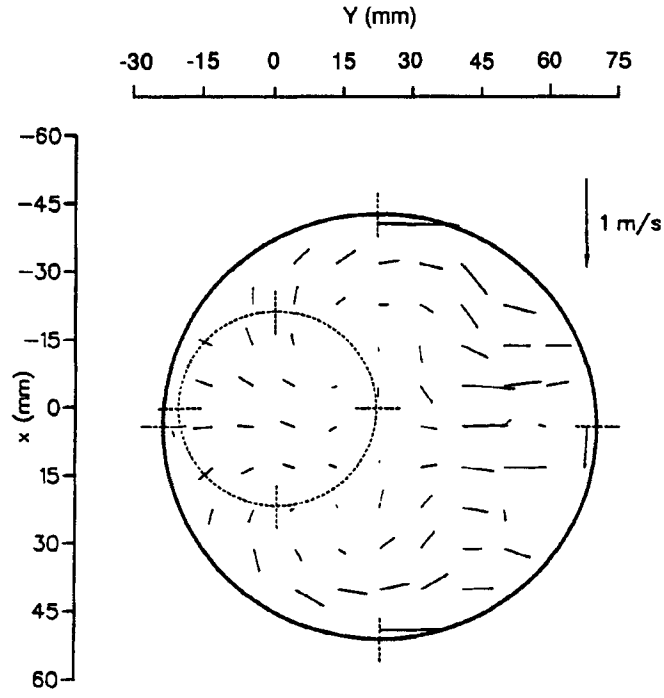

Figure 5. Measured mean velocity vectors in $z = -25$ mm plane ($L = 6$ mm, $Re = 25{,}760$)

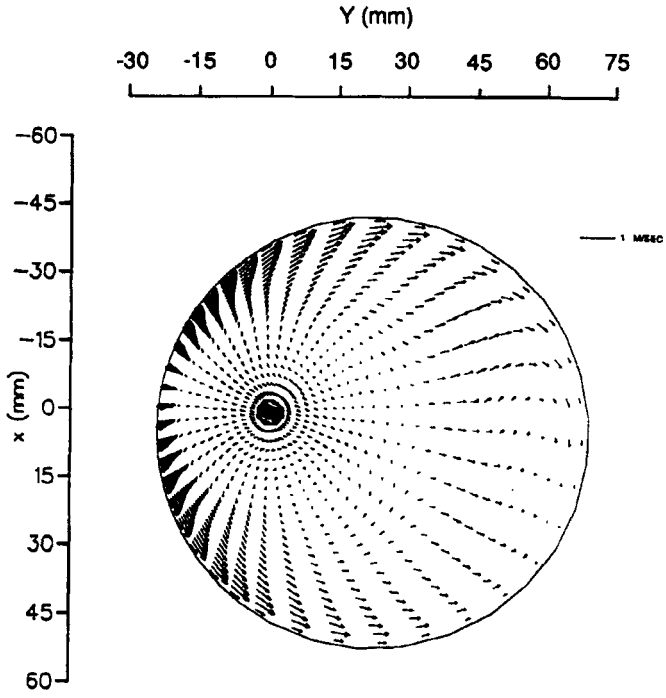

Figure 6. Predicted mean velocity vectors in $z = -25$ mm plane ($L = 6$ mm, $Re = 25{,}760$)

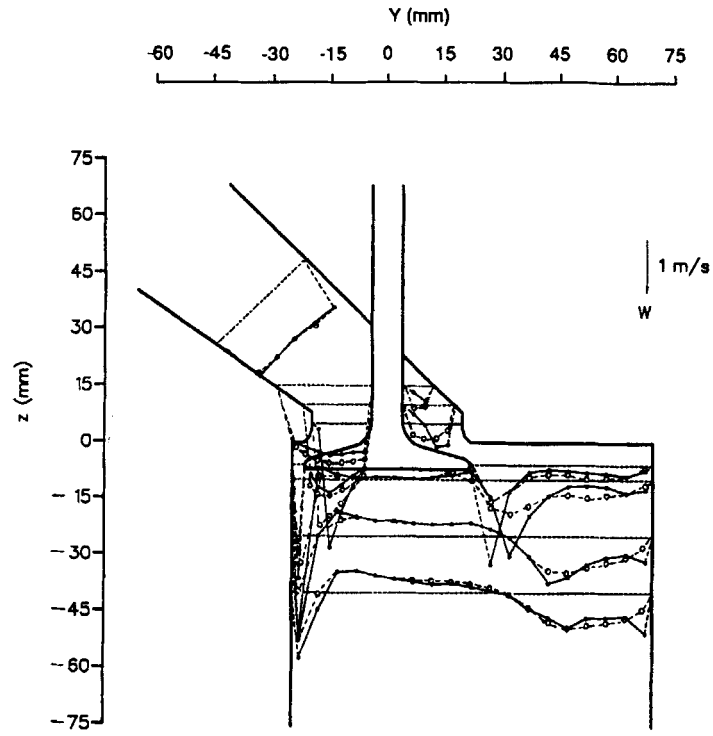

Figure 7. Comparison of measured and predicted profiles of axial mean velocity component in $x = 0$ mm plane ($L = 6$ mm, $Re = 25{,}760$): —— ● ——, measurements; — — ○ — —, predictions

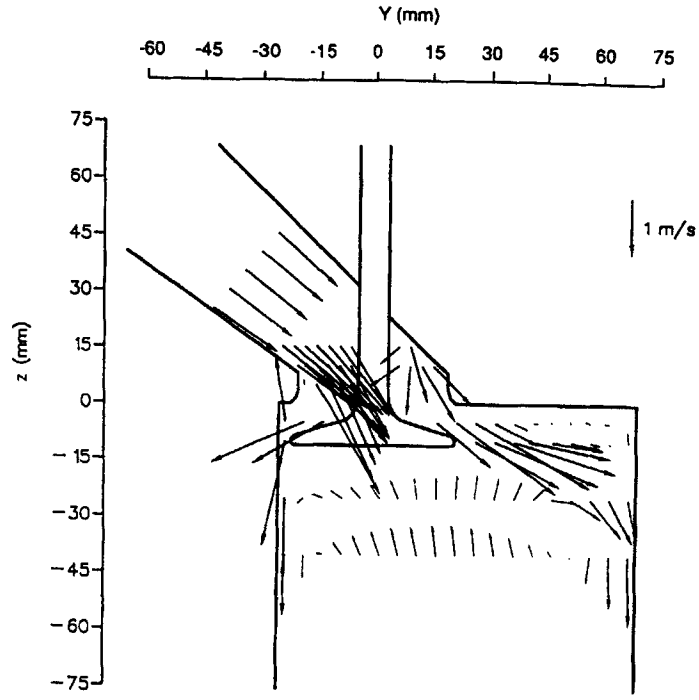

Figure 8. Measured mean velocity vectors in $x = 0$ mm plane ($L = 10$ mm, $Re = 25{,}760$)

flow impinging on the left-hand-side cylinder wall, that nearest to the valve, is deflected sideways to form two counter-rotating vortices, one on each side of the x-axis. Both streams move along the cylinder periphery from left to right. As the valve axis is offset from the cylinder axis in the x-direction, the flow velocities on the top side of the figure are larger, resulting in the flow near the right side of the cylinder being directed towards the bottom of the figure. This feature is shown by both the LDA and CFD results.

The above comparisons of the predictions and experimental data show that the simulation not only reproduced all the important features of the flow but also provided more detailed information and more extensive identification of the flow features revealed by the LDA data. Overall there is excellent qualitative agreement between experiment and calculation in both the z–y and x–y planes.

Quantitative comparisons of the predictions and experimental data are shown in Figure 7, where profiles of the axial mean velocity component in the $x = 0$ mm plane are presented. Upstream of the valve stem the predicted axial velocity profile is in extremely good agreement with the measured one. In the $z = 10$ and 15 mm planes upstream of the valve stem, where the flow is accelerating and directed towards the valve stem by the port, the axial velocity is overpredicted by 10%.

The experiments showed that the small separation region adjacent to the wall and above the valve seat is located at $z = 5$ mm. However, the axial velocities near the wall at $z = 5$ mm are overpredicted and there is no evidence of a local recirculation in the CFD results. Conversely, the peak velocity in the same profile is underpredicted by around 20%. Further calculations with a locally refined grid yielded practically identical results and it might be concluded that the failure to predict this recirculation is not caused by insufficient grid resolution, as discussed further below.

On the right of the valve stem the predicted axial velocity profiles overestimate the velocities near the stem and underestimate them in the vicinity of the port wall. Inside the cylinder there is very good quantitative agreement between the LDA and CFD results in most locations. The only exceptions are found in the profiles at $z = -5$ and -10 mm, where the peaks on the right side of the valve, although

located at exactly the same y-positions in both experiment and simulation, are considerably underpredicted. It should be noted, however, that further downstream the profiles are nearly identical across most of the plane.

Mean flow structure, 10 mm valve lift

The second valve lift selected for investigation was 10 mm, to ensure that the flow characteristics were sufficiently different from the intermediate lift of 6 mm described above. Mean velocity vectors in the z–y planes are shown in Figures 8–11, in the same order of presentation as in the preceding subsection, and quantitative comparisons of LDA and CFD velocity profiles are shown in Figure 12.

The velocity profiles upstream of the valve stem (Figure 8) are very similar to the 6 mm results of Figure 3, indicating that the flow in this region is independent of the valve lift. This finding is in agreement with earlier studies of both production and axisymmetric ports.[10] The flow separation on the left of the stem is more extensive than for the 6 mm lift, as indicated by the larger angle of the flow to the valve axis, and extends into the cylinder, where a large reverse velocity was measured next to the valve curtain area. However, the reverse velocities immediately downstream of the port ramp are again very small and can be barely distinguished in the diagram. Downstream of the valve stem the vectors are larger than for the 6 mm lift, indicating a more pronounced separation in the wake of the stem.

On the left side of the cylinder the jet is directed more sharply towards the wall at this higher valve lift. This is primarily caused by the presence of the aforementioned larger recirculation along the left side of the port; as the flow bypasses this recirculation, it is sharply deflected by the valve crown. The vortex in the top left corner of the cylinder and the ring vortex beneath the valve are larger than for the 6 mm lift.

On the right side of the valve the jet enters the cylinder in this case at a 30° angle to the cylinder head, compared with the 38° angle with the 6 mm lift. This is caused primarily by the larger separation region on the left side upstream of the valve seat mentioned earlier. In addition, it was observed in the flow visualization tests and has been reported in earlier studies[4,12] that there is a more pronounced separation region on the valve head at higher lifts, the effect of which is to direct the inlet jet at a

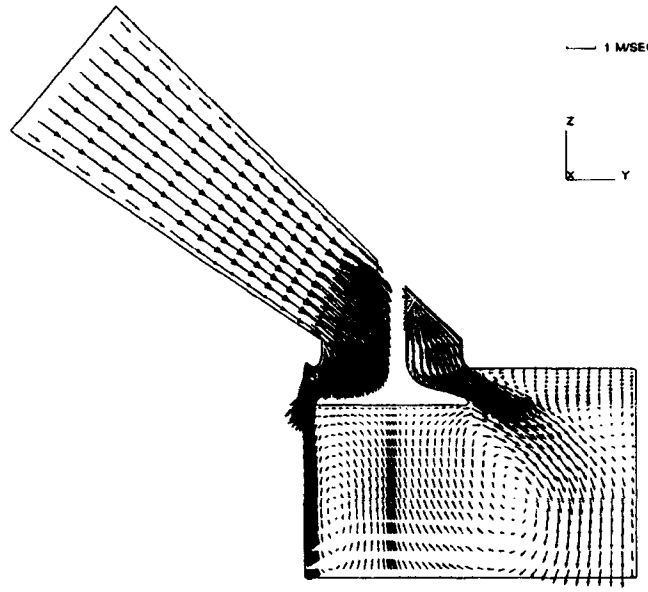

Figure 9. Predicted mean velocity vectors in $x = 0$ mm plane ($L = 10$ mm, $Re = 25{,}760$)

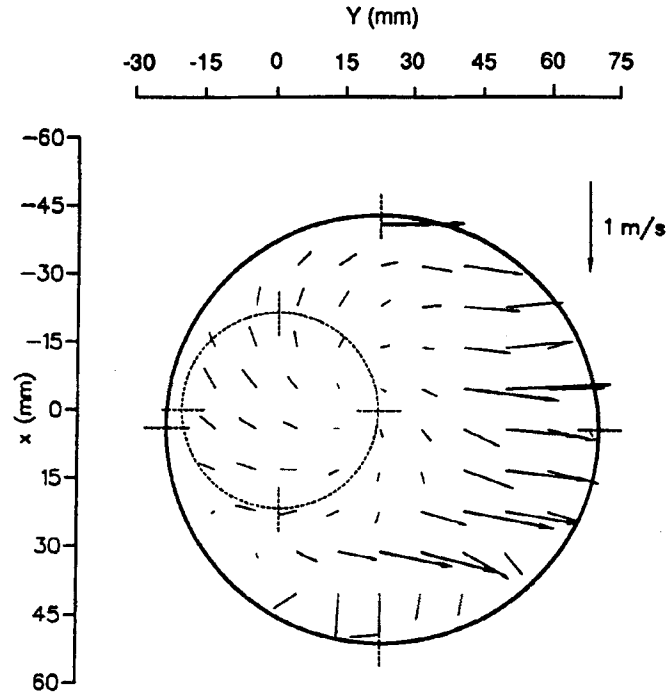

Figure 10. Measured mean velocity vectors in $z = -25$ mm plane ($L = 10$ mm, $Re = 25{,}760$)

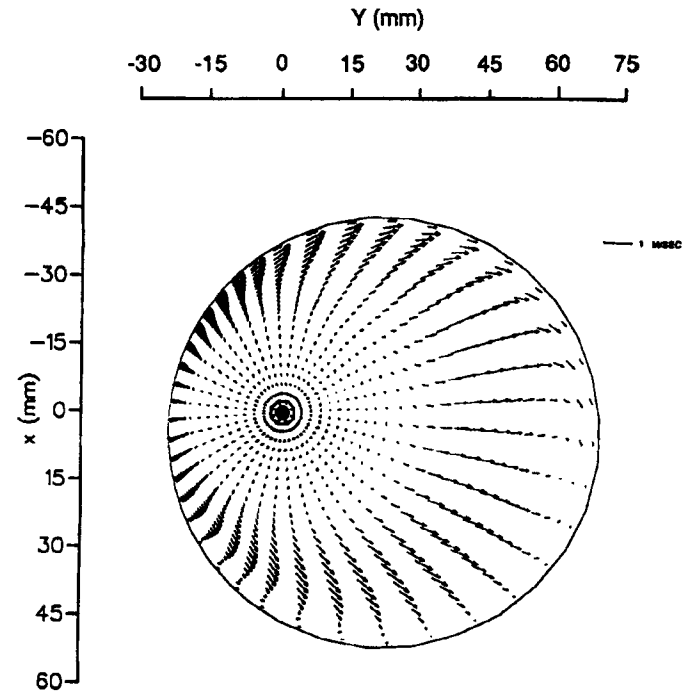

Figure 11. Predicted mean velocity vectors in $z = -25$ mm plane ($L = 10$ mm, $Re = 25{,}760$)

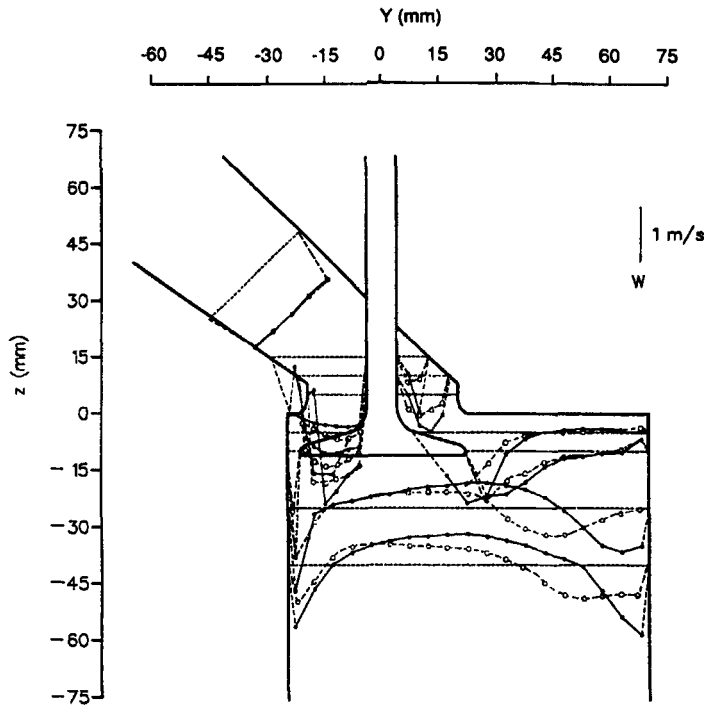

Figure 12. Comparison of measured and predicted profiles of axial mean velocity component in $x = 0$ mm plane ($L = 10$ mm, $Re = 25{,}760$): —— • ——, measurements; — — o — —, predictions

smaller angle to the cylinder head. This effect is strongly dependent on port shape and it has been reported that with conventional directed (curved) ports the angle of the jet in relation to the cylinder head increases with valve lift.[17]

The inlet jet penetrates to the right wall, where it is deflected in part upwards to generate a counterclockwise-rotating vortex along the cylinder head. Most of the jet mass is deflected downwards, however, forming another vortex beneath the valve which rotates in the opposite direction.

The predicted velocity vectors (Figure 9) show a flow structure very similar to that of Figure 8. The flow at the stem wake is well predicted, as is the toroidal vortex beneath the valve, which is more symmetrical than that present with the 6 mm lift. The two recirculations on the left and right sides of the cylinder head are also well predicted. However, the flow reversal on the left side of the port is not shown in the CFD results and the predicted flow remains attached until the middle of the valve seat. One important implication of this is that the jet on the right of the valve is at a larger angle to the cylinder head than in the experiment (see Figure 8).

In the horizontal (x–y) plane, Figure 10, the flow structure is considerably different from that with the 6 mm lift. Underneath the valve a clockwise-rotating swirl flow is present. The inlet jet issuing from the valve is evident, as indicated by the large velocities directed towards the right of the figure. A third feature is the smaller clockwise circulation near the bottom of the figure. All flow motions are present in the predicted vectors (Figure 11), but the size of the last circulation is underpredicted. As for the 6 mm lift, there is good qualitative agreement in both planes presented and all major flow features have been predicted.

The quantitative comparisons of the LDA and CFD velocity profiles in Figure 12 show, however, more discrepancies between experiment and calculation compared with the 6 mm lift results. There is good agreement upstream in the port and the magnitudes of the measured and calculated velocities in

the cylinder are similar in many locations. However, the peak velocities of the jet on the wall of the cylinder are again underpredicted and the locations of the maxima on the right side of the cylinder are different.

Comparing the 6 and 10 mm lift LDA and CFD results, it might be concluded that the main, if not the only, reason for the discrepancy is that the small recirculation on the left side of the port is not predicted. It is evident from the experiments that the separation becomes more extensive as the valve lift is increased. Consequently the inlet jet is deflected more significantly with increasing lift, resulting in larger discrepancies between prediction and measurement. Whereas with the 6 mm lift the measured and predicted jet angles differed by only 0·5°, the predicted angle to the cylinder head with the 10 mm lift is 3° larger than the measured one. As a result, the peak velocities at $z = -20$ and -40 mm are located 15 mm nearer the valve axis than the measured ones.

In conclusion, differences in the predicted and measured mean flow structures appear to stem from this small recirculation, which in the higher-lift predictions seems to alter the trajectory of the jet by 3°. Although this may have only a small effect on the overall development of the flow in an engine cylinder, possible reasons for this discrepancy are assessed below.

Turbulence level and kinetic energy distributions, 6 and 10 mm valve lifts

Predicted distributions of the kinetic energy of turbulence, $k = \frac{1}{2}(u'^2 + v'^2 + w'^2)$, are shown in contour form for the valve lifts of 6 and 10 mm in Figures 13 and 14 respectively. The distributions are qualitatively similar at both valve lifts. There are major quantitative differences though: for example, the maximum value of k predicted for the 6 mm lift is 0·123 $m^2\ s^{-2}$, approximately 50% higher than the 0·064 $m^2\ s^{-2}$ maximum obtained with the 10 mm lift. This difference might be expected, as there are steeper velocity gradients present in the flow at lower lift. The two figures show, however, that more extensive regions of high k are present with the higher lift. The shapes of these regions show that turbulence is generated primarily at the shear layers at the edges of the jets issuing into the cylinder and near the valve crown where the flow impinges and is redirected.

An assessment of the overall level of turbulence in the flows can be made by considering the volume-averaged values of k, which were calculated in the manner described in Section 3. These were 0·0235 and 0·0229 $m^2\ s^{-2}$ for the 6 and 10 mm valve lifts respectively, a difference of under 3%. It

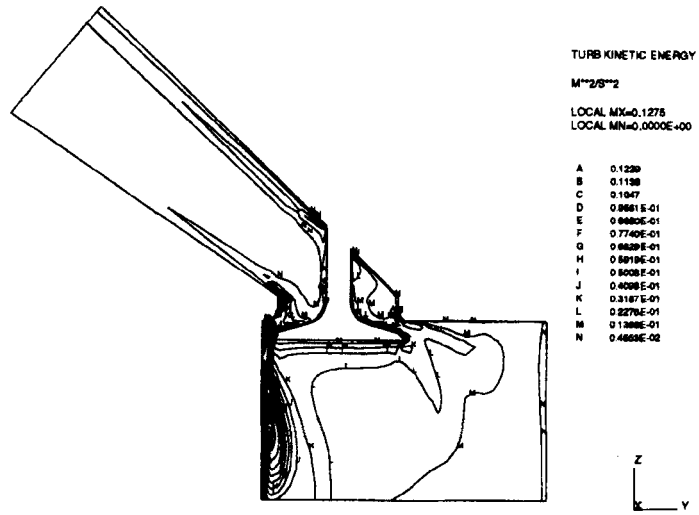

Figure 13. Predicted contours of turbulent kinetic energy in $x = 0$ mm plane ($L = 6$ mm, $Re = 25{,}760$)

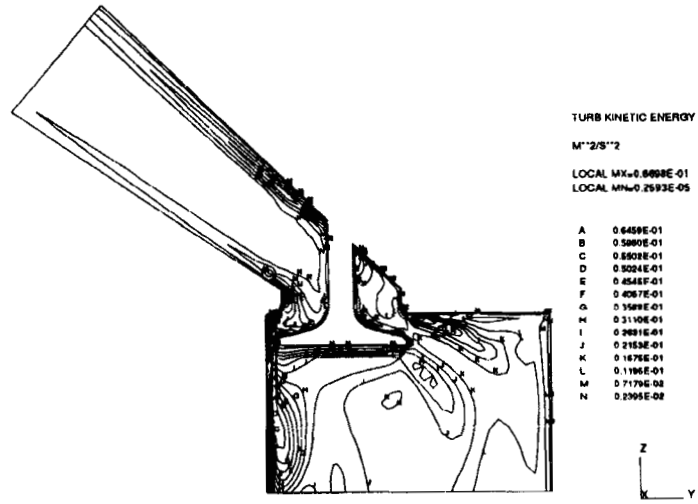

Figure 14. Predicted contours of turbulent kinetic energy in $x = 0$ mm plane ($L = 10$ mm, $Re = 25{,}760$)

would be interesting to relate the volume-averaged kinetic energy with the level of tumble produced under different valve lift conditions. However, the shape of the measured and predicted velocity profiles in the present work is such (see e.g. Figure 7) that calculation of the tumble ratio using the normally employed definition is not possible without significant approximations.

Comparisons between the measured and predicted turbulence levels cannot be made directly, as the

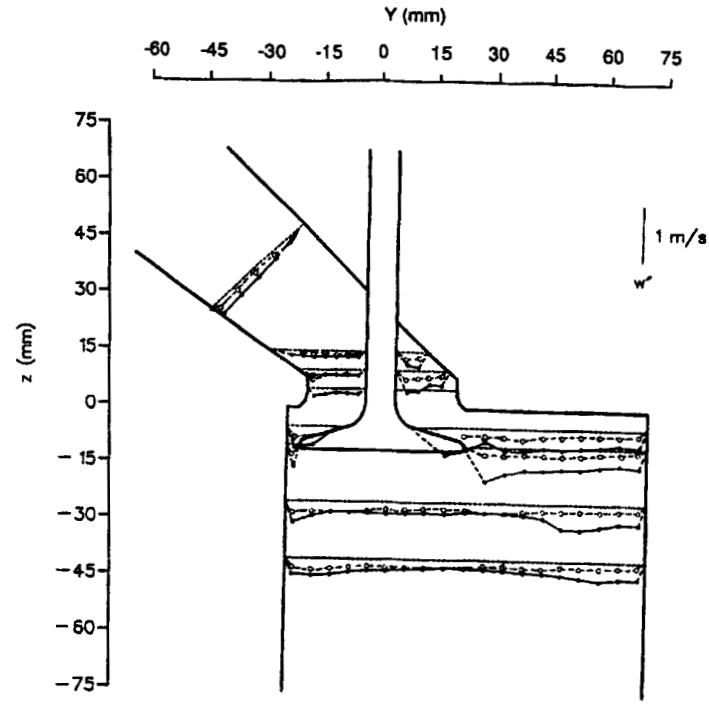

Figure 15. Comparison of measured and predicted profiles of axial RMS velocity component in $x = 0$ mm plane ($L = 10$ mm, $Re = 25{,}760$): —— ● ——, measurements; — — ○ — —, predictions

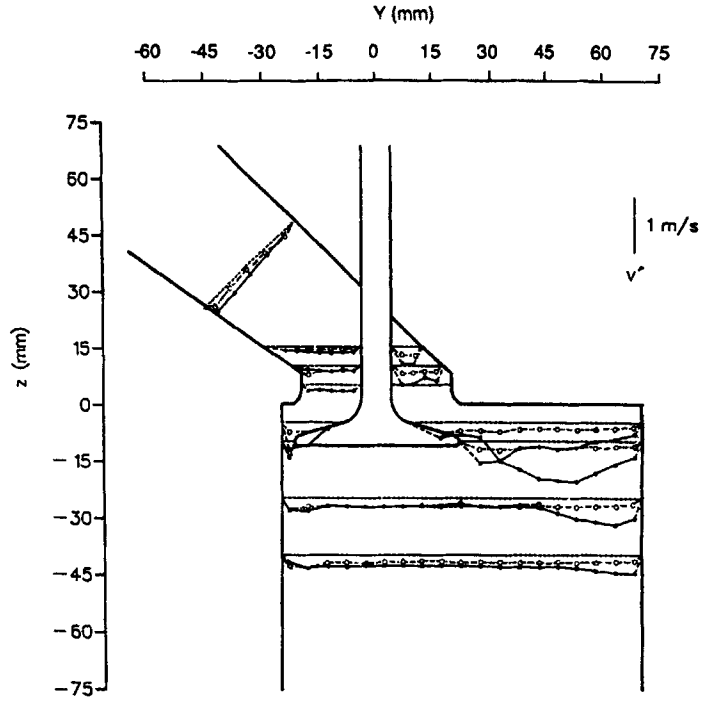

Figure 16. Comparison of measured and predicted profiles of radial RMS velocity component in $x = 0$ mm plane ($L = 10$ mm, $Re = 25{,}760$): —— • ——, measurements; — — o — —, predictions

k–ε model of turbulence employed here does not predict the three normal stresses (turbulence levels) separately. However, an assessment can be made if isotropic turbulence is assumed, in which case $u' = v' = w' = (2k/3)^{0.5}$. It should be noted that in the standard version of the k– ε model employed in this work, the formulation of the model makes use of the same eddy viscosity ν_t for the three normal components of the Reynolds stress, i.e. u', v' and w', and therefore there is an implicit assumption of locally isotropic turbulence.[18]

Comparisons of the measured and predicted (calculated as $(2k/3)^{0.5}$) profiles of w' and v' for the 10 mm valve lift are shown in Figures 15 and 16. The measured and predicted profiles are qualitatively similar in many parts of the flow, the most evident exception being the jet flow region on the right of the cylinder. There are quantitative differences between experiment and simulation over parts of the flow field. In these parts the fluctuating velocity profiles are consistently underpredicted, especially in the jet flow region on the right of the cylinder. Good quantitative agreement between experiment and prediction is found across two-thirds of the cylinder diameter in the two profiles beneath the valve.

Although the above comparisons between the measured v' and w' and the calculated $(2k/3)^{0.5}$ involve an approximation, they nevertheless provide an indication of the accuracy of the predictions. The main shortcoming of the simulation is the underprediction of the turbulence levels, which was noted above to be particularly significant in the vicinity of the intake jet.

One main reason for the above differences was identified from the flow visualization tests. The intake jet was observed to be flapping intensely on one side of the cylinder (the right side in Figures 15 and 16). This flapping behaviour has been observed in previous studies of both steady[11] and motored[19] engine flows. As a result, ensemble-averaged RMS velocity or turbulence level measurements in the region of intake jets include the variation in the mean velocity with time due to the jet flapping. This results in a broadening of the RMS velocities measured, as the variation in the mean velocity is

interpreted as a higher turbulence level. The flapping was observed to be more pronounced in the y-direction and this is partly reflected in the values of v' being greater than those of w' in that vicinity.

Therefore it is more appropriate to obtain time-resolved LDA measurements in such regions so that the variation in the mean flow with time can be accounted for. This is normally achieved by removing low-frequency fluctuations from the time-resolved velocity variation by means of FFT techniques.[20] Care must therefore be exerted when CFD results are compared with ensemble-averaged LDA data. RMS values used for comparison purposes should be obtained through time-resolved measurements from which the mean flow variation has been removed. This problem is not found exclusively in internal combustion engine flows; a mean velocity variation is also present in, for example, rotating impeller flows and the effect on the ensemble-averaged RMS levels is similar.[21]

The turbulence levels are underpredicted in other regions of the flow where jet flapping has no effect. However, the differences between measured and predicted values in these regions are significantly smaller (by almost an order of magnitude) than in the jet vicinity. Such differences may be partly attributed to stem from the assumption of isotropy implicit in the standard k–ε model formulation mentioned earlier. It has been suggested[22] that of predictions reported which employed the k–ε model, those which made use of a three-dimensional non-isotropic version of the model provided the most realistic simulation of the flow field. Comparison of the measured profiles of w' and v' in locations away from the intake jet in Figures 15 and 16 shows, however, that although the two components are by no means identical, they are similar in magnitude. Therefore away from the jet region the assumption of isotropy might not be expected to be the major source of discrepancy.

It is generally accepted that the standard k–ε model does not predict well the behaviour of shear layers subject to adverse pressure gradients, streamline curvature and rapid acceleration and a number of flow modellers have reported discrepancies between experimental data and predictions obtained from numerical schemes employing this model.[23]

It is interesting to note that in earlier predictions of steady flow through an axisymmetric port,[24] agreement between experiment and simulation was better at the higher lift. This was attributed to the presence of a small recirculation region along the valve seat at the lower lift which was not predicted, even though the local grid resolution was around 0·25 mm. The presence and size of such small recirculation regions on the valve seat/head depend on the valve lift.[12] Further improvement in CFD predictions of inlet port flows is therefore critically dependent on the ability to predict such small-scale flow features, which may have a considerable influence on the flows further downstream.

One source of uncertainty may be the inlet conditions employed for the calculations. The geometry upstream of the test section was identical with that used in the simulation and the mean velocities specified seem to be appropriate, as is evident from the comparisons in Figures 7 and 12. The level of k and the length scale specified at the inlet were chosen in accordance with recommendations of earlier CFD studies of engine flows.[2] Measured inlet length scale values are not available, but the value specified here (4·6 mm) is comparable with those measured inside other ports of similar size.[20]

Although improvements through (extensive) further grid refinement cannot be dismissed, the discrepancies observed above are expected to stem primarily from the lack of modelling of the flapping of the intake jet and shortcomings of the turbulence model, especially in flow regions where the turbulence is anisotropic and there is strong streamline curvature. As the data show that u', v' and w' are not equal in parts of the flow, the use of Reynolds stress turbulence models which do not assume local isotropy might be expected to yield more accurate predictions.

Influence of mass flow rate

In order to determine the influence of the mass flow rate on the flow structure, predictions were also carried out for the 10 mm valve lift for two other mass flow rates, 0·898 and 1·539 kg s^{-1}, i.e. 65%

and 112% of the flow rate used for the predictions reported above. The mean flow and turbulence structures were qualitatively identical and results at the other flow rates are not shown here for economy of presentation. The mean velocities scaled perfectly with the flow rate. The calculated values of the volume-averaged turbulence kinetic energy corresponding to mass flow rates of 0·898, 1·379 and 1·539 kg s^{-1} were 0·0093, 0·0229 and 0·0289 m^2 s^{-2}. These average k-values scale with the square of the ratio of the flow rates concerned. Similarly, local values of k scaled with the square of the flow rate ratio across the flow field.

These results showed that the flow pattern through the port and in the cylinder is independent of the mass flow rate. This confirms the findings of earlier LDA studies of flows through curved and straight port designs,[11] which showed that the ensemble-averaged mean and RMS velocities for different flow rates, normalized by the bulk velocity, were nearly identical for most flow rates; differences were only observed at very low flow rates, where it is expected that parts of the flow may not be fully turbulent and such comparisons are therefore not appropriate.

Comparison of predictions with and without modelling the port shape

The generation of the mesh for the port shape was the most complex and time-consuming part of the present numerical simulation procedure. In addition, in many port designs the direction of the flow entering the cylinder is not dissimilar to that of the port centreline. It is important for design purposes to determine whether the port centreline shape can be used as a good indicator of the direction of the flow entering the cylinder; if predictions of acceptable accuracy can be obtained by specifying only that the direction of flow entry is that of the port centreline upstream of the valve seat, then decisions on port shape can be made early in the design process and optimization of the less influential port features can then follow. In order to examine whether the need for modelling the complete port could be alleviated, a comparison of flow predictions made with and without modelling the port shape was performed for the valve lift of 10 mm.

In the absence of the port model the inlet velocities were specified to be of uniform magnitude, calculated from the mass flow rate of 1·379 kg s^{-1} and the local cross-sectional area. The inlet flow was specified to enter the cylinder at 40° to the cylinder head, which is identical with the angle of the port centreline.

Figures 17 and 18 present the flow structure in the cylinder with and without the inlet port respectively. The inlet plane for the latter case is the horizontal plane shown as a full line upstream of the valve. The predicted mean flow structures are similar

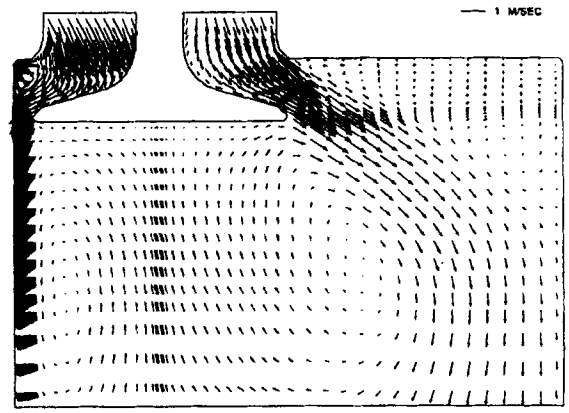

Figure 17. Predicted mean velocity vectors in $x = 0$ mm plane ($L = 10$ mm, $Re = 25{,}760$); port shape modelled

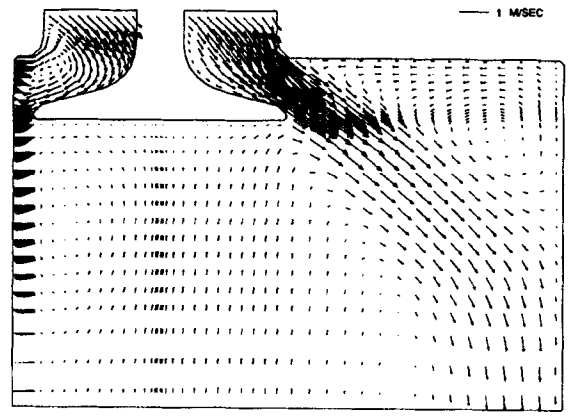

Figure 18. Predicted mean velocity vectors in $x = 0$ mm plane ($L = 10$ mm, $Re = 25{,}760$); port shape not modelled

in the two cases, but a number of local differences can be observed. First, the recirculation region on the left of the stem is more extensive when the port shape is not modelled. This might be expected owing to the proximity of the inlet plane where the 40° flow direction was specified. The redirection of the flow due to the large separation results in a smaller part of the flow entering the cylinder on the left side of the valve and therefore the velocities along the left wall are smaller in Figure 18.

Second, the wake of the stem on the right of the valve is not predicted, as might be expected, when the port shape is not modelled. Following from this, the direction of the intake jet on the right of the valve is different; the angle of this jet to the cylinder head is larger in Figure 18. Consequently the shape of the ring vortex beneath the valve is different. For example, the centre of the right part of the vortex in Figure 18 is located further away from both the cylinder head and the axis than in Figure 17. Clearly the accuracy of the predictions is reduced and their agreement with the experimental data (where the intake jet angle was 30°) is poorer when the port shape is not modelled.

Differences in the distribution of k are expected, due to the differences in the predicted mean flow fields, and were observed (these results are not shown for economy of presentation). However, the values of the volume-averaged turbulent kinetic energy were similar: 0·0229 $m^2\ s^{-2}$ with and 0·0224 $m^2\ s^{-2}$ without the port. Notwithstanding the reduced accuracy of the CFD simulations which do not account for the port shape, the similarity of the flow fields in Figures 17 and 18 indicates that calculations using the port centreline shape to specify the flow direction close to the valve seat may be useful as a first approximation. This method should prove effective to select between ports with different centreline shapes and thus minimize the effort involved in port design optimization, but must be followed by predictions modelling the complete port.

6. CONCLUDING REMARKS

The major conclusions that can be drawn from the present study are as follows.

1. The main features of the steady flow produced in a cylinder downstream of a generic port with a straight centreline are an annular intake jet surrounded by two ring vortices—a larger one located beneath the valve and a smaller one in the periphery of the cylinder head. The intake jet was observed to flap considerably.
2. An increase in the valve lift from 6 to 10 mm resulted in significant differences in the mean flow in the cylinder, but there was no noticeable effect on the flow in the port upstream of the valve stem.

3. The mean flow and turbulence kinetic energy distributions scaled well with the flow rate through the port.
4. In general the CFD predictions of the mean velocities and k were in good qualitative agreement with the LDA data; good quantitative agreement was obtained between measured and predicted mean velocities in many parts of the flow. In general the LDA and CFD results were similar, except where the flow is influenced by a small recirculation region in the port which was not reproduced in the simulation. The underprediction of k in the vicinity of the intake jet was attributed to the flapping of the jet, which was not accounted for in the simulation.
5. It was shown that simulations made by assuming the flow entering the cylinder to follow the direction of the port centreline can provide a useful first approximation of the flow field. With the port shape modelled in full, the accuracy of the predictions is improved and such detailed modelling will be necessary for port shape optimization.

ACKNOWLEDGEMENTS

The authors acknowledge support from the EPSRC under grant GR/J65693 and from Ford Motor Company for the work reported in this paper.

REFERENCES

1. J. B. Heywood, *Internal Combustion Engine Fundamentals*, McGraw-Hill, New York, 1988.
2. A. D. Gosman, Y. Y. Tsui and C. Vafidis, 'Flow in a model engine with a shrouded valve—a combined experimental and computational study', *SAE Paper 850498*, 1985.
3. T. Yamada, T. Inoue, A. Yoshimatsu, T. Hiramatsu and M. Konishi, 'In-cylinder gas motion of multi-valve engines—three-dimensional numerical simulation', *SAE Paper 860465*, 1986.
4. A. F. Bicen, C. Vafidis and J. H. Whitelaw, 'Steady and unsteady airflow through an intake valve of a reciprocating engine', *Proc. ASME Winter Ann. Meet.*, New Orleans, LA, December 1984, ASME, New York, 1984.
5. W. Brandstätter, R. J. R. Johns and G. Wigley, 'The effect of inlet port geometry on in-cylinder flow structure', *SAE Paper 850499*, 1985.
6. M. Errera, J. Labbe and A. Jerot, 'Three-dimensional numerical analysis of in-cylinder flow in an internal combustion engine', *SAE Paper 880106*, 1986.
7. D. C. Haworth, S. H. El Tahry, M. S. Huebler and S. Chang, 'Multidimensional port-and-cylinder flow calculation for two- and four-valve-per-cylinder engines: influence of intake configuration on flow structure', *SAE Paper 900257*, 1990.
8. K. Naitoh, H. Fujii, T. Urushihara, Y. Takagi and K. Kuwahara, 'Numerical simulation of the detailed flow in engine ports and cylinders', *SAE Paper 900256*, 1990.
9. S. Aita, A. Tabbal, G. Munck, N. Montmayeur, Y. Aoyagi, Y. Takenaka and S. Obana, 'Numerical simulation of swirl port–valve–cylinder flow in diesel engines', *SAE Paper 910263*, 1991.
10. M. J. Tindal, R. S. W. Cheung and M. Yianneskis, 'Velocity characteristics of steady flows through engine inlet ports and cylinders', *SAE Paper 880383*, 1988.
11. R. S. W Cheung, S. Nadarajah, M. J. Tindal and M. Yianneskis, 'An experimental study of velocity and Reynolds stress distributions in a production inlet port under steady flow conditions', *SAE Trans. J. Eng.*, **100**, 334–353 (1991).
12. L. S. Kastner, T. J. Williams and J. B. White, 'Poppet inlet valve characteristics and their influence on the induction process', *Proc. Inst. Mech. Eng.*, **178**, 955 (1963–1964).
13. M. Yianneskis, R. S. Cheung and M. J. Tindal, 'A method of investigating flows in inlet ports of complex shape, *Proc. Int. Conf. on Combustion Engines—Technology and Applications*, London, May 1988, Institution of Mechanical Engineers, London, 198x, pp. 51–58.
14. *STAR-CD Version 2.112*, Computational Dynamics Limited, 1991.
15. B. E. Launder and D. B. Spalding, 'The numerical computation of turbulent flows', *Comput. Methods Appl. Mech. Eng.*, **3**, 269–289 (1974).
16. S. V. Patankar and D. B. Spalding, 'A calculation procedure for heat, mass and momentum in three-dimensional parabolic flows', *Int. J. Heat Mass Transfer*, **15**, 1787–1805 (1972).
17. J. C. Dent and A. Chen, 'An investigation of steady flow through a curved inlet port', *SAE Paper 940522*, 1994.
18. M. B. Abbott and D. R. Basco, *Computational Fluid Dynamics: An Introduction for Engineers*, Wiley, New York, 1990.
19. K. O. Suen, M. J. Tindal and M. Yianneskis, 'Characteristics of the flow in the vicinity of an intake valve of a diesel engine', *Proc. Third Int. Conf. on Laser Anemometry—Advances and Applications*, Swansea, September 1989, pp. 47.2–47.12.

20. M. Yianneskis, M. J. Tindal and S. Nadarajah, 'Measurement of turbulence scales, moments and spectra in engine flows', *Proc. Institution of Mechanical Engineers Second Seminar on Experimental Methods in Engine Research and Development*, London, December 1991, Institution of Mechanical Engineers, London, 199x, pp. 127–133.
21. K. Van't Riet, W. Bruijn and J. W. Smith, 'Real and pseudo-turbulence in the discharge stream from a Rushton turbine', *Chem. Eng. Sci.*, **31**, 407–412 (1976).
22. G. B. Tatterson, *Fluid Mixing and Gas Dispersion in Agitated Tanks*, McGraw-Hill, New York, 1991.
23. R. A. Issa and A. D. Gosman, 'The computation of 3D turbulent two-phase flows in mixer vessels', *Proc. 2nd Int. Conf. on Numerical Methods in Laminar and Turbulent Flows*, Venice, 1981.
24. Z. Lilek, M. Peric, S. Nadarajah, M. J. Tindal and M. Yianneskis, 'Measurement and simulation of the flow around a poppet valve', *Proc. Eighth Turbulent Shear Flows Symp.*, Munich, September 1991, pp. 13.2.1–13.2.6.